Study of Bi2Sr2CaCu2O8/BiFeO3 nano-composite for electrical transport applications

S. Acharya, A. K. Biswal, J. Ray, and P. N. Vishwakarma

Citation: J. Appl. Phys. **112**, 053916 (2012); doi: 10.1063/1.4751277
View online: http://dx.doi.org/10.1063/1.4751277
View Table of Contents: http://jap.aip.org/resource/1/JAPIAU/v112/i5
Published by the American Institute of Physics.

Study of $Bi_2Sr_2CaCu_2O_8/BiFeO_3$ nano-composite for electrical transport applications

S. Acharya, A. K. Biswal, J. Ray, and P. N. Vishwakarma[a)]
Department of Physics, NIT-Rourkela, Odisha 769008, India

(Received 16 June 2012; accepted 9 August 2012; published online 10 September 2012)

The $Bi_2Sr_2CaCu_2O_8/BiFeO_3$ (BSCCO/BFO) nano composite for various BFO weight percentage is prepared and studied for electrical transport. Double resistive superconducting transition is seen in all composite samples with increasing semiconducting nature as a function of BFO content. Initially, the added BFO goes mainly to the grain boundary and from 10% onwards, it enters grains as well, acting as pinning centers. The conduction mechanism in BSCCO shows weak localization for low BFO, tunneling in intermediate BFO, and power law behavior (similar to metal-insulator boundary) for higher BFO samples. The paraconductivity studies reveal the 2D-3D transition in parent BSCCO and the composites, with a signature of percolative behavior in the composites. The study of critical current density reveals two types of Josephson junction in the composites: (1) thin intrinsic superconductor-insulator-superconductor (SIS) type present in all samples including parent BSCCO and (2) extrinsic type due to BFO added, present only in composite samples. The extrinsic junction is SIS with tunneling for low BFO and goes to proximity SIS type for increasing BFO. The Jc(0) as a function of BFO content, first decreases with increasing BFO, attains minima at 5% BFO, and increases thereafter. © *2012 American Institute of Physics*. [http://dx.doi.org/10.1063/1.4751277]

I. INTRODUCTION

Even after several decades of research on high Tc superconductors, these materials are still interesting for many researchers. Recent interest in these materials is to combine them with ferromagnetic, ferroelectric, etc. materials for new insights and device applications.[1–3] The multilayer structure of superconductor with other oxides, in particular, multilayers of high Tc cuprates and colossal-magnetoresistance manganites, has been paid special attention. Investigation of pulsed laser deposited $YBa_2Cu_3O_7/La(Sr)MnO_3$ bilayers reveals the long scale proximity effect between YBCO and LSMO layers.[4] Localized penetration of superconductivity into the $La_{0.7}Ca_{0.3}MnO_3$ up to distances much larger than that is possible for Cooper pairs in a singlet spin state to exist is[5] observed in $La_{0.7}Ca_{0.3}MnO_3$ films epitaxially grown on $Pr(Ce)CuO_4$.

Besides the above mentioned applications, one of the most promising and basic applications of superconductors is in the electrical power transport. Hence, there has been consistent effort in the enhancement of current carrying capacity, which may be achieved by incorporating extended defects acting as pinning centers. The effect of pinning centers is at its best when their sizes are of the order of coherence length. It has been shown that the introduction of high density YBCO 211 nano particles (size 15 nm) on the multilayers of ultrathin YBCO 211 and 123 increases the critical current (at 77 K) by a factor of two to three for high magnetic fields.[6] For the enhancement of current density, it is also important that the density of these pinning centers should be as high as $10^{11}\,cm^{-2}$. Many times in order to achieve these large densities, large numbers of defects are also created which degrades the superconducting properties. Recently, it was found that magnetic nano-particles may act as efficient pinning centers at much lower density.[7,8] Since then various magnetic nano-particles pinning centers in superconductors have been investigated.[9–12] In recent years, $BiFeO_3$ (BFO) has emerged as potential candidate for various applications due to its large magneto-electric coupling.[13] The ground state of BFO is antiferromagnetic, however, its nano form exhibits superparamagnetism,[14] which is very suitable for pinning effect in superconductors. In this paper, we explore the possibility of using BFO as pinning centers in $Bi_2Sr_2CaCu_2O_8$ (BSCCO-2212). Besides pinning effects, the conduction mechanism in these materials is also investigated. So far, very few work has been reported on BSCCO with magnetic nanoparticles. Moreover, BSCCO has elemental similarity with BFO. The 2212 phase of BSCCO is chosen because it can be synthesized without lead doping (which is non-eco friendly), which otherwise is essential for 2223 phase of BSCCO.

II. EXPERIMENTAL

The BSCCO 2212 phase is prepared from high purity Bi_2O_3, $SrCO_3$, $CaCO_3$, and CuO by solid state reaction method. The powder mixture is heated to 700 °C for 12 h, 770 °C for 12 h, and 800 °C for 20 h with intermediate grinding at every stage. The resultant powder is made pellet and kept for sintering at 880 °C for 12 h. Synthesis of nano-BFO is done via sol-gel assisted auto combustion route using Bi $(NO_3)_3{\cdot}5H_2O$ and Fe $(NO_3)_3{\cdot}9H_2O$ as precursors. Glycine is used as chelating agent/fuel for this purpose. The metal ions:glycine ratio is maintained as 1:1. The solution containing all the precursors is heated under constant stirring till the solution turns into brown colored gel and ultimately burnt

a)Electronic mail: prakashn@nitrkl.ac.in.

vigorously resulting in a brown color powder. The brown powder is then calcined at 700 °C for 1 h to get BFO.

Desired amount of BSCCO and BFO powders is taken in various weight ratios and grinded for 20–30 min for homogeneous intermixing. Then, the mixed samples were made pellet of 10 mm diameter and kept for final heat treatment at 800 °C for 10 min. In this way, the nano-composite of 1%, 2%, 3%, 4%, 5%, 10%, 15%, 20%, 25%, and 30% BFO in BSCCO is prepared.

III. RESULT AND DISCUSSION

One of the pellets after the final sintering is crushed into powder and analyzed via x-ray diffraction. The x-ray diffraction results shows the composite nature, i.e., separate peaks corresponding to the BSCCO and BFO phases (Fig. 1). Small amount of 2201 phase is also seen. No shift in the peak position is observed, indicating no structural modification due to inclusion of BFO nano particles. The peaks corresponding to BFO are not visible for the lower concentration of BFO (<5%) and are apparent only after 5% and above.

Temperature dependence of resistance (R-T) below room temperature is done by four probe method using constant current source (Keithley 2161) and nano-voltmeter (Keithely 2182), in a closed cycle refrigerator. The electrical contacts over the samples (thickness $\sim$ 1 mm) are made with the help of conducting silver epoxy. To obtain the true sample voltage, the voltage measurement is done for current reversal as well, which minimizes the thermoelectric voltage.

The temperature dependence of resistivity for all the samples is shown in Fig. 2, as normalized resistivity with respect to 273 K, ρ/ρ_{273}. The behavior of BSCCO is almost linear as the sample is cooled from room temperature. Transition to superconducting state begins at the $T_{c\text{-}on}$ and is complete (when resistance becomes completely zero) at T_{C0}. The mean field transition temperature, T_c is obtained from

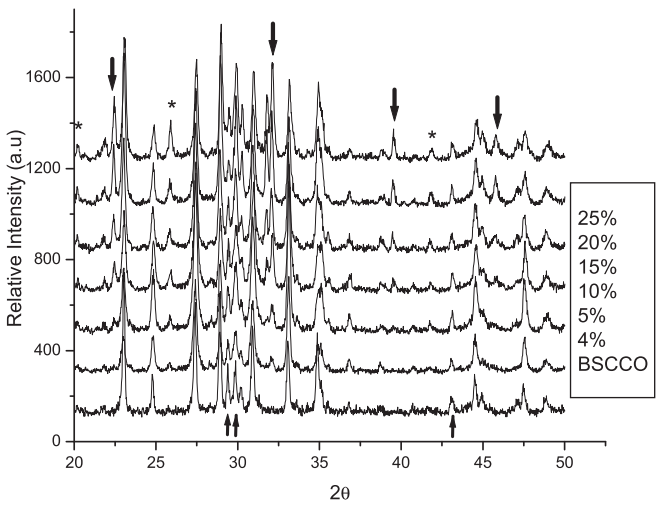

FIG. 1. X-ray diffraction plot of BSCCO/BFO composite. The plots are slightly off-shifted for better clarity. The peaks marked up arrow ↑ represents 2201 phase and those marked down arrow ↓ represents $BiFeO_3$ phase. Some extra peaks in composite samples marked (*) is observed which resembles with Bi free superconducting phase $Ca_7Sr_7Cu_{24}O_{41}$ (JCPDS: 48-1503).

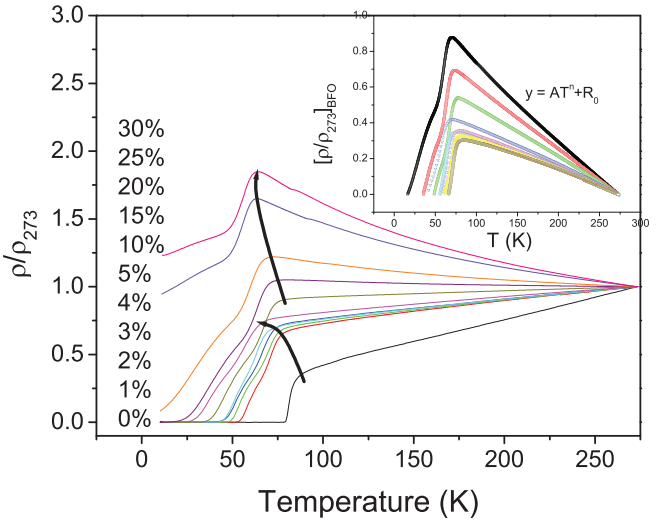

FIG. 2. Temperature variation of normalized resistivity ρ/ρ_{273} for BSCCO and its composites with BFO (1%, 2%, 3%, 4%, 5%, 10%, 15%, 20%, 25%, and 30%). The two arrows show the variation of $T_{c\text{-}on}$ with increasing BFO concentration in the sample. The inset shows the temperature dependence of normalized resistivity (ρ/ρ_{273}) of BFO in the sample. This resistivity is found to obey the power law $\rho^{gb} \propto T^n$. $[\rho/\rho_{273}]_{BFO} = [\rho/\rho_{273}]_{sample} - [\rho/\rho_{273}]_{BSCCO}$.

the derivative of resistance vs. temperature, i.e., dR/dT. The addition of BFO in BSCCO induces non-linearity in the normal region of ρ-T data and with increasing BFO content, the semiconducting nature increases, which is very clear as negative temperature coefficient of resistance for higher BFO concentration (after 10% BFO) samples.

The onset of superconductivity, $T_{c\text{-}on}$ as a function of BFO concentration is shown by joining the respective $T_{c\text{-}on}$ via arrows in Fig. 2. One interesting fact which is noticed from this plot is that, though the $T_{c\text{-}on}$ decreases with BFO addition, but the trend of decrease in $T_{c\text{-}on}$ is of two types: a converging behavior upto 5% BFO and a diverging behavior for 10% onwards. One more point noticed for all BSCCO/BFO composites is that the superconducting transition temperature splits in two (revealed as double peak in the dR/dT data), T_{C1} and T_{C2}, along with a broadening of overall superconducting transition temperature. Such behavior is accounted to the weak-link nature of granular superconductors as the later is composed of superconducting grains embedded in a nonsuperconducting host.[15] Of the two superconducting transitions temperatures, the higher one marks the superconductivity in grains whereas the grain boundary still remains normal and the lower one when the grain boundary also becomes superconducting. Transition at T_{C1} manifests significant amount of strongly coupled grains and the zero resistance state is achieved when the Josephson tunneling between the grains forms a connected superconducting path across the entire sample at T_{C2} as the temperature is lowered. With increasing concentration of BFO, both the transition temperatures shift to lower values, but the shift in T_{C2} is found to be more rapid than T_{C1} (shown in Table I). The appearance of additional transition temperature T_{C2} and its broadening clearly reflects that the BFO added, goes to the grain boundary region, and becomes superconducting only due to proximity effect at lower temperatures.[16] With

TABLE I. Variation of superconducting parameters with BFO wt. %. Samples having BFO% more than 15, did not show zero resistance, hence not included here.

BFO conc.	$T_{c\text{-}on}$ (K)	T_{c1}(K)	T_{c2}(K)	T_{c0}(K)	ΔT_{c1}(K)	ΔT_{c2}(K)
0%(BSCCO)	90.74	81.07	81.07	80.24	10.5	…
1%	83.47	70.63	57.72	53.14	18.78	11.55
2%	81.96	70.06	53.46	47.79	20.11	14.06
3%	81.64	66.92	51.16	46.18	20.72	14.74
4%	79.08	63.58	50.61	43.42	22.74	12.92
5%	78.81	56.83	36.81	37.77	24.08	16.96
10%	81.53	67.6	44.34	34.16	24.25	23.12
15%	77.43	63.73	36.55	20.24	24.4	32.79

increase in BFO, the grain boundary due to it increases and T_{C0} decreases very rapidly to the lower temperature. At 10% BFO, a sudden increase in T_C, T_{C1}, and T_{C2} is seen. For higher concentrations of BFO (more than 10%), the transition temperature again decreases but its trend is different from the earlier decrease (see Fig. 3). This decrease is because of increasing non-superconducting phase in the sample which ultimately leads to the decay of superconductor ordering. From Fig. 3, it is clearly seen the two different trends of monotonically decrease in transition temperature for lower (up to 5 wt. %) and higher (>5%) BFO concentration.

With further increase in BFO concentration, the metallic BSCCO ultimately falls below the percolation threshold and an incomplete transition at T_{C2} is observed (see Fig. 1 for 30%, 25%, and 20% BFO added samples). Intergranular broadening (ΔT_{c2}) is found to be increasing due to addition of BFO where as intrinsic width (ΔT_{c1}) increases initially for 1% and then remains almost constant.

Though the superconductivity is apparent at $T_{c\text{-}on}$, the processes leading to it starts much earlier to this temperature, $\approx 2T_{c\text{-}on}$.[17] This temperature is called pseudo gap temperature (T*). Below this temperature, the resistivity deviates from its normal behavior and decreases slightly faster than its usual behavior. The temperature dependence of resistivity for parent BSCCO in the region 150–300 K is found to be well described by a linear behavior $\rho(T) = \rho(0) + \alpha T$. Hence, any deviation from this behavior is marked as due to onset of T*. To obtain T*, the temperature dependent of resistivity data is plotted as $[\rho(T) - \rho(0)]/\alpha T$. At the onset of T*, $[\rho(T) - \rho(0)]/\alpha T \neq 1$, which otherwise is one.[18] For the composites, the exact nature of the grain boundaries introduced by BFO is not known, hence a slightly different procedure is employed to obtain T*. A best polynomial fit is done for parent BSCCO. Then, this value is subtracted from the resistivity data of all composites to obtain the resistivity variation of BFO alone. In this way, the resistivity behavior of BFO grain boundaries in the samples is obtained. The temperature dependence of resistivity in these grain boundaries is found to obey a simple power law, $\rho^{gb}(T) \propto aT^{\alpha}$ shown in the inset of Fig. 2. Hence, for BSCCO/BFO composites, the T* is obtained by locating the temperature at which $[\rho(T) - \rho(0) - \rho^{gb}(T)]/\alpha T \neq 1$. As a function of BFO composition, the T* thus obtained are (see Fig. 4) 178, 124, 115, 131, 117, 104, 124, 100 K for BSCCO, 1%, 2%, 3%, 4%, 5%, 10%, 15% BFO added samples, respectively. Hence, the overall effect of insertion of BFO in BSCCO is to decrease T*.

To have a better insight of BSCCO-BFO interface in the composite system, analysis of normal state resistivity is done in detail. Since the grain boundaries have disordered nature until a critical concentration of BFO (~5%) is reached, it is much plausible to consider the weak localization theory for disordered media as the conduction mechanism for the low BFO sample.[19] According to the weak localization theory, the temperature dependence of resistivity follows $T^{1/2}$ behaviour at high temperature (T > 100 K).[20] Hence, ρ-T plot is fitted with $\rho(T) = \rho(0) + aT + bT^{1/2}$ above $T_{c\text{-}on}$. The first term is the residual resistivity, the second term is linear metallic behavior as seen in parent BSCCO, and last term ($T^{1/2}$) is due to weak localization. It can be seen in the plot that the fitting is reasonably good, which supports weak localization conduction mechanism. However, the fit is found to be good only till 10% BFO (Fig. 5). For 15% BFO,

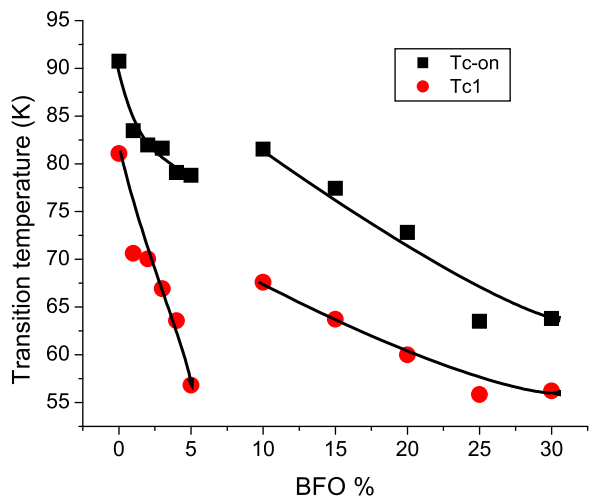

FIG. 3. Plot of on-set transition temperature $T_{c\text{-}on}$ and mean field transition temperature T_{c1}, obtained from the dR/dT plot, as a function of increasing BFO content in the sample. The lines are just a guide to eye.

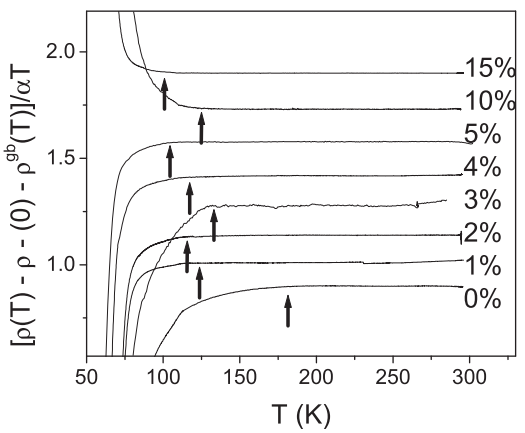

FIG. 4. Plot of $[\rho(T) - \rho(0) - \rho^{gb}(T)]/\alpha T$ as a function of temperature. Deviation from the flat behavior marks the onset of pseudogap temperature T* (shown as arrow mark). The respective plots are off-shifted for better clarity.

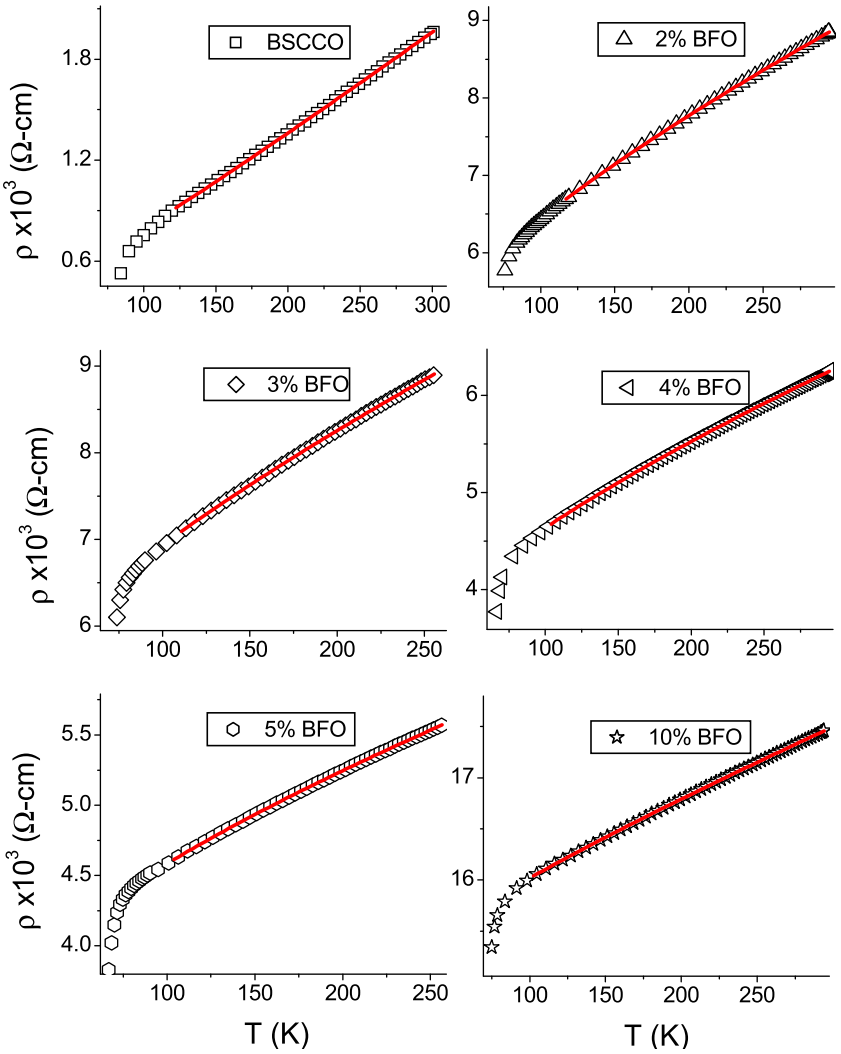

FIG. 5. ρ-T plot is found to be good fit with $\rho(T) = \rho(0) + AT + BT^{1/2}$ up to 10% BSCCO/BFO. The solid lines are the fit corresponding to the equation.

the resistivity behavior is found to be better fitted with $\log\rho T^{-1/2}$ (Fig. 6), a behavior similar as tunneling through grain boundaries in granular metals.[21,22] Considering the granular nature of our samples, we too ascribe this behavior to the tunneling of carriers through the grain boundary. For higher concentration of BFO (20%, 25%, and 30%), ρ-T plots are found to have good fit with $\rho(T) \propto T^{-\beta}$ (Fig. 6) proposed by Macmillan[23] and Larkin and Khmel'nitskii[24] for the samples on the boundary of metal-insulator transition or critical region. The exponent takes the value $0.33 < \beta < 1$, with $\beta \sim 0.33$ on the metallic side and $\beta \sim 1$ on the insulating side. However, experimentally, the values of β beyond the above range have also been reported and have been ascribed towards the metallic side ($\beta < 0.33$)[25] and the insulating side of the boundary ($\beta > 1$).[26] In our samples, the respective values of exponents are 0.12, 0.15, and 0.22 for (20% BFO, 25% BFO, and 30% BFO), respectively. These values of exponent indicate that the samples are towards metallic side of the M-I boundary and with increasing BFO concentration, the behavior is shifting towards insulating. Hence, the parent BSCCO is metallic in nature and with increasing BFO content, the sample drift towards insulating side via critical regime. However, the insulating regime is not reached even for 30% BFO added sample.

In the case of conventional superconductor, while cooling, zero resistance appears suddenly at the superconducting transition temperature, T_c. But in case of HTSC, the initiation of thermodynamic fluctuations much before the transition temperature gives rise to an anomalous increase in superconducting properties even at temperature above T_c. This fluctuations induced conductivity is less than the normal state conductivity by a factor $\frac{1}{k_F^2 \ell \xi(0)}$ which comes out to be $\sim 10^{-5}$ for conventional (type I) superconductors, where k_F is the Fermi wave vector and ℓ is the mean free path.[27] However, for type II superconductors, the coherence length $\xi(0)$ is large, and hence the excess conductivity is no longer small. The study of this fluctuation induced conductivity provides a great deal of information such as coherence length, dimensionality of conduction, and dimensionality cross-over (if present).[28]

The fluctuation induced excess conductivity or paraconductivtiy ($\Delta\sigma$) in the above temperature range is obtained by

$$\Delta\sigma = \sigma_m - \sigma_n, \tag{1}$$

where σ_m is the measured conductivity and σ_n is the extrapolated conductivity drawn above the $2T_c$. Actually, the

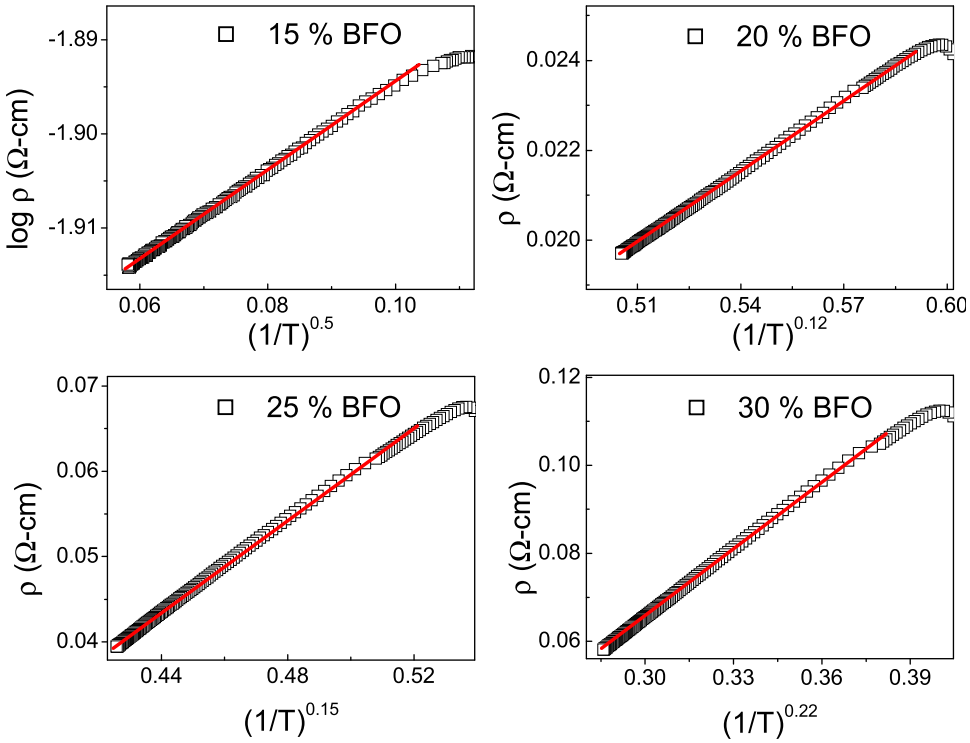

FIG. 6. For 15% BFO, temperature dependence of resistivity is fitted with $\log\rho \propto T^{-1/2}$ and $\rho(T) \propto T^{-\beta}$ for 20%–30% BFO composite samples. The solid lines are the fit to the respective equations.

resistivity is measured first and it is converted to conductivity via $\sigma = 1/\rho$.[29]

Aslamazov and Larkin provide the following expressions for excess conductivity in the paraconductivtiy region,[27]

$$\Delta\sigma = A\varepsilon^{\lambda} = A\varepsilon^{-(4-D)/2}, \tag{2}$$

where ε is the reduced temperature $\varepsilon = (T–T_C)/T_C$ and "D" is the dimensionality parameter.

Here, T_c is mean field critical temperature (obtained from the derivative of R-T data) and λ is a dimensionality parameter. More elaborately,

$$\text{For 3D case, } \Delta\sigma_{3d} = \frac{1}{32}\frac{e^2}{\hbar\xi(0)}\varepsilon^{-0.5}, \tag{3}$$

$$\text{For 2D case, } \Delta\sigma_{2d} = \frac{1}{16}\frac{e^2}{\hbar d}\varepsilon^{-1}, \tag{4}$$

TABLE II. Various parameters obtained from the paraconductivity studies of BSCCO/BFO composites: 2D-3D cross-over temperature T_0, 3D and 2D exponents λ_{3D} and λ_{2D} or $\lambda_{percolative}$, Coherence length (ξ) and Josephson coupling constant (E_J). 20% sample is not included here as the T_{C2} is not available.

Conc of BFO	T_0 (K)	λ_{3D}	[λ_{2D}] λ_{perco}	ξ_C (Å)	(E_J)
0%(BSCCO)	85.12	−0.47	[−0.94]	1.67	0.19
1%	73.66	−0.41	−1.61	3.94	1.10
2%	72.86	−0.41	−1.31	4.51	1.45
3%	70.53	−0.5	−1.24	4.61	1.51
4%	66.63	−0.41	−1.37	4.21	1.26
5%	61.03	−0.42	−1.75	6.07	2.62
10%	70.57	−0.38	−1.53	5.76	2.36
15%	66.66	−0.42	−1.52	6.80	3.29

$$\text{For 1D case, } \Delta\sigma_{1d} = \frac{1}{16}\frac{e^2\xi(0)}{\hbar S}\varepsilon^{-3/2}, \tag{5}$$

where $\xi(0)$ is the coherence length at $T = 0$ in the stacking direction of multilayer structure, d is the superconducting layers periodicity length, and S is the cross sectional area of 1D conductor.

In the layered superconductor, the superconducting properties are highly anisotropic. The mobility in the CuO_2 conduction plane depends on the charge reservoir layers $MBa_2O_{4-}\delta$ (M = Y, Bi, Hg, Ti, etc.). The charge reservoir layers are known to supply the carriers to the conducting plane where the superconductivity occurs. In order to reach the CuO_2 plane, the charge carriers have to overcome each time the thickness of charge reservoir layer barrier which is mostly resistive. When the superconductivity starts at $T_{c\text{-}on}$, the cooper pairs are confined only to CuO_2 plane and hence the superconductivity is 2D in nature.[30] The charge carrier from the reservoir crosses the layer barrier only, when the temperature is further lowered. At this point, the superconductivity is spread in the entire crystal; hence its nature is 3D. A careful observation of excess conductivity as a function of temperature often reflects the transition from 2D to 3D, as one approaches T_c from high temperature.[28]

Once knowing the cross over temperature (T_0), the other parameters such as coherence length (ξ_C) and Josephson coupling constant (E_J), (see Table II) may be calculated as per Lawrence and Doniach (LD) model[31]

$$T_0 = T_C[1 + (2\xi_C/d)^2] \tag{6}$$

and

$$E_J = (2\xi_C/d)^2. \tag{7}$$

The LD model is a model for Josephson-coupled superconducting-insulating superlattices. Our samples are in powder form rather than a multilayer. Therefore, one would expect the LD model to only capture the qualitative aspects of our data and not to be relevant in a quantitative sense. In order to study the excess conductivity in our samples, the data are plotted as $\ln(\Delta\sigma) - \ln(\varepsilon)$ (shown in Fig. 7). Two distinct changes in slope for each plot have been observed with gradual increase in temperature. The slope value gives the value of λ; hence in order to know it, the two regions are linearly fitted. The exponent value $\lambda \sim -0.5$ indicates 3D fit and $\lambda \sim -1$ corresponds to 2D fit. The cross over temperature (T_0) is calculated by finding the common solution for the two linear fit equations.

In the as prepared BSCCO sample, λ_{3D} is found to be -0.47 and λ_{2D} is -0.94, which fits well with the theoretical value. The cross over temperature is found to be 85.12 K. For the BSCCO/BFO composites, the respective values of exponent determined from these plots are $\lambda \sim -0.5$ and $\lambda \sim -1.5$. Value of $\lambda \sim -1.5$ gives an impression of 1D nature of conduction. However, similar values have also been found in films having percolative conduction.[32] Using numerical simulations technique, Seto *et al.*[33] have shown that for inhomogeneous superconductors, the exponent takes the value $\lambda = 1.33$. With the composite nature of our samples, the $\lambda \sim -1.5$ is attributed to the percolative conduction due to inhomogeneity in composite samples.

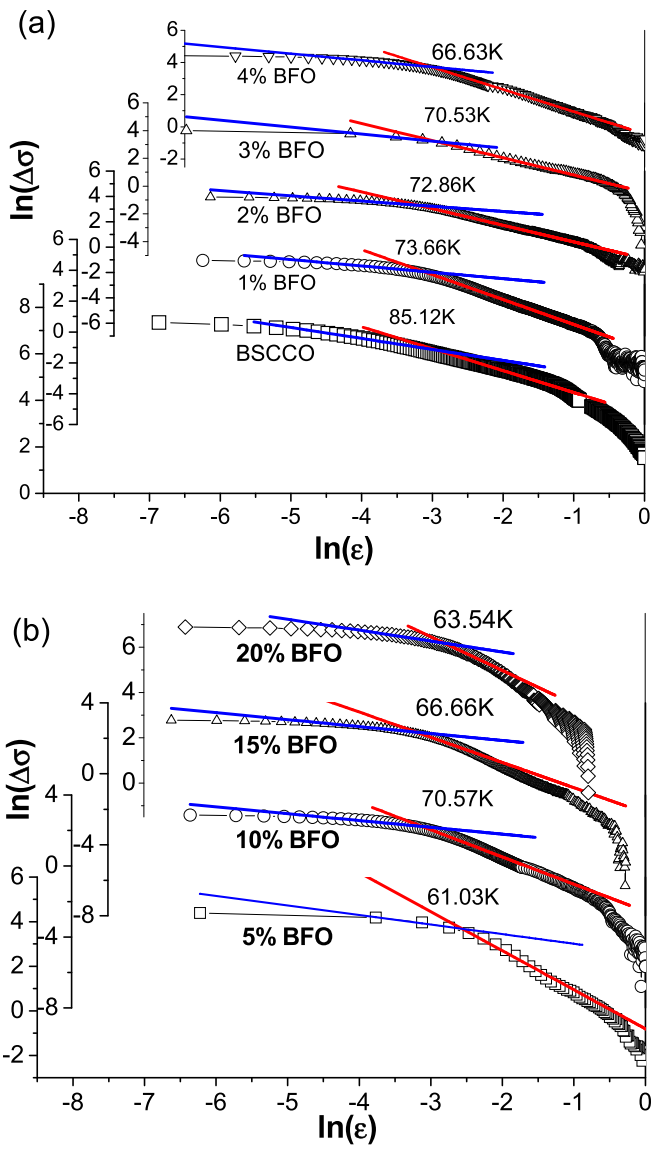

FIG. 7. ln ($\Delta\sigma$) vs. ln (ε) plot of BSCCO and its composites (a) 1%, 2%, 3%, 4% (b) 5%, 10%, 15%, and 20% added BFO. 2D and 3D fitted regions are shown by straight lines along with cross over temperature at the intersection of solid lines.

The cross-over temperature T_0 so obtained is monotonically decreasing with increase in BFO content. The decrease is continuous till 5%, increases for 10% by ~10 K and again decreases. This observation is again similar to the earlier observation of T_C, where low concentration of BFO added to BSCCO, goes to the grain boundary region and enters the grain as pinning centers only for 10% and above.

Once knowing the cross-over temperature T_0, coherence length ξ_C is calculated using $T_0 = T_{C0}[1 + (2\xi_C/d)^2]$, where d is the thickness of superconducting layer (15 Å) and for T_C, T_{C2} is taken because at T_{C2} grains as well as grain boundaries become superconducting.

The critical current density (J_c) is obtained from the critical current as $J_c = I_c/A$, where A gives cross sectional area of the rectangular bar sample. The critical current I_c is obtained from the V-I characteristics at a fixed temperature. In all the V-I plots, no voltage is observed, until a critical value of current I_C is reached, at which a non-zero voltage starts appearing. Beyond this value, the voltage increases non-linearly initially and then becomes linear. This measurement is repeated at temperature intervals of 5 K below the critical temperature, till the lowest temperature 6 K. In this way, the critical current I_C for various temperatures is obtained. The entire set of experiments is done for all the samples including parent BSCCO. It must be mentioned here that the I_C value measured for 10% BFO and 15% BFO at 6 K is beyond the limit of our current source, which is 105 mA. Hence, I_C at 6 K for these two samples is considered as 110 mA. But in any case, the value of parameter "n" would not be less than the observed one. The critical current I_C thus obtained is converted to critical current density J_c by using the relation $J_c = I_c/A$. This temperature dependence of critical current density is fitted to $J_c(T) = J_c(0)(1 - T/T_c)^n$. The exponent "n" takes the values depending on the type of Josephson junction and is n = 2 for superconductor–normal metal–superconductor (SNS) junction,[34] n = 1 for

TABLE III. Values of critical current density $J_c(0)$ and "n" in the two regions.

	Region 1		Region 2	
Conc. of BFO	$J_c(0) \times 10^3$ in A cm^{-2}	n	$J_c(0) \times 10^3$ in A cm^{-2}	n
0% (BSCCO)	75.81	0.42	…	…
2%	55.62	0.2	58.71	0.08
3%	41.43	0.39	50.97	0.04
4%	44.9	0.41	44.9	0.41
5%	30.24	0.49	43.77	0.54
10%	20.27	0.55	141.95	2.44
15%	25.44	0.36	297.99	2.01

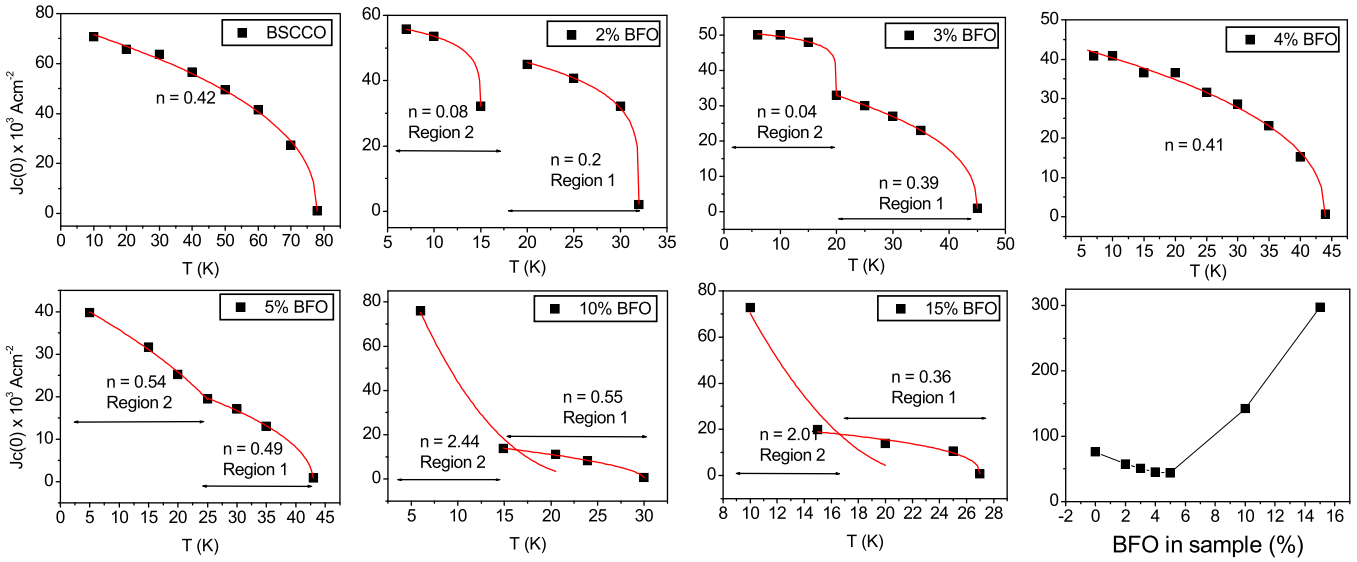

FIG. 8. Variation of critical current density (J_c) as a function of temperature (T). The solid red lines are fit to the equation $J_c(T) = J_c(0)(1 - T/T_c)^n$ in the respective regions. Plot of $J_c(0)$, obtained from the fitting of above equation in region 2, as a function of BFO content in BSCCO is shown in the last figure. Here, the solid black line is just a guide to eye.

superconductor–insulator–superconductor (SIS) junction.[35] If the SIS junction is thin enough so that the quasiparticles may tunnel through it, then $n = 0.5$.[36]

While fitting the above equation to the J_c-T plot, it is found that the data for parent BSCCO fit very well in the entire temperature range with $n = 0.42$, which is very close to the value predicted for the tunneling through thin SIS junctions. For BSCCO/BFO composites, the equation fits in two different regions (region 1 and region 2) with different values of "n" in the respective region (Table III).

The region near the T_c (region 1) still holds $n \sim 0.5$, where as the temperature approaches $T = 0$ (hence called as region 2), the value of "n" diverges from 0.05 to 2 while going from 2% BFO to 15% BFO, respectively (Fig. 8). Hence, from these results, it seems that the grain boundary of the composites is of two kinds (see Fig. 9). The first kind of grain boundary is the intrinsic kind having the parent BSCCO composition but in disordered form. This grain boundary is very thin and is present in all samples including parent BSCCO. The second kind of grain boundary is formed when BFO is introduced in the sample. This grain boundary is having composition of BFO and is very thin and disordered for lesser BFO content (the value of $n = 0.05$, indicating tunneling through Josephson junction). As the BFO content is increased, the thickness of this grain boundary increases and the junction becomes SNS type ($n \sim 2$). But being insulating nature of BFO, SNS junction seems confusing. It has been shown by Golubov *et al.*[37] that $n = 2$ for SIS junction is possible under strong proximity effect. In the temperature dependence of resistivity, we have already seen that BFO contribution to resistivity is not insulating but is of critical behavior due to proximity effect. Hence, $n = 2$ behavior due to proximity effect is quite reasonable. A plot of $J_c(0)$ obtained as the intercept of the above equation fitting in the low temperature range (region 2) as a function of BFO content in the sample is shown in Fig. 8. From the plot, it is evident that the J_c first decreases on BFO incorporation in the sample, attains a minimum value at 5% BFO and increases thereafter. This is because, for higher values of BFO, the BFO goes not only in the grain boundary region but also enters inside the grain.[38] The BFO nano particles inside the grain act as pinning centers and hence an increase in J_c is observed. It must be mentioned here that the observed Jc is not as high as the earlier reported values, but still this study enables us to examine the other aspects which would not have been possible for high J_c samples, due to instrumental limitations. Moreover, most of the reported high J_c is obtained indirectly via magnetization measurements, where grain boundaries effects are not prominent.[39] Grain boundaries are an inevitable part of any superconductor produced in large scale. Hence, for any transport based practical applications, the actual value is a better choice rather than the indirect one.

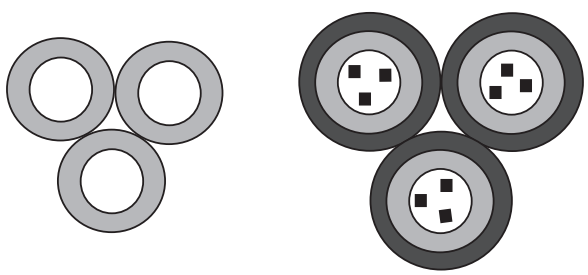

FIG. 9. Schematic grain/grain boundary arrangement for BSCCO/BFO composites. The inner most circles are the superconducting grains and second one with light shade are the intrinsic grain boundaries. The additional grain boundary due to BFO (shown with dark shade circle) is present in second figure. The dark spots in the second figure stand for the BFO nano particles inside the grains acting as pinning centers.

IV. CONCLUSIONS

In conclusion, BSCCO/BFO composites show metallic to insulating behavior with increasing weight percentage of BFO in BSCCO. Initially, the BFO added contributes to the grain boundary and from 10% onwards, it enters grains as

well. Action of BFO as pinning centers happens only after 10%, but simultaneously this also brings insulating behavior. Insertion of BFO in BSCCO introduces an additional SIS type Josephson junction which is under strong proximity effect. The critical current density $J_c(0)$ as a function of BFO content decreases initially till 5% and increases thereafter. After summarizing all these findings, the 10% BSCCO/BFO samples is found to be ideal for electrical transport based applications because of its metallic conduction and high $J_c(0)$.

ACKNOWLEDGMENTS

The authors wish to thank DST, India and BRNS (Mumbai), India for project support. The authors J.R. and A.K.B. would like to thank UGC-DAE CSR Indore and BRNS, India, respectively, for the fellowship and financial assistance. Professor Sunil Kumar Sarangi is acknowledged for his encouragement and support.

[1]L. R. Tagirov, Phys. Rev. Lett. **83**, 2058 (1999).
[2]A. Crassous, R. Bernard, S. Fusil, K. Bouzehouane, D. Le Bourdais, S. Enouz-Vedrenne, J. Briatico, M. Bibes, A. Barthélémy, and J. E. Villegas, Phys. Rev. Lett. **107**, 247002 (2011).
[3]G. P. Pepe, L. Parlato, N. Marrocco, V. Pagliarulo, G. Peluso, A. Barone, F. Tafuri, U. Scotti di Uccio, F. Miletto, M. Radovic, D. Pan, and R. Sobolewski, Cryogenics **49**, 660 (2009).
[4]J. G. Lin, D. Hsu, M. Y. Song, C. H. Chiang, and W. C. Chan, J. Appl. Phys. **107**, 09E130 (2010).
[5]Y. Kalcheim, O. Millo, M. Egilmez, J. W. A. Robinson, and M. G. Blamire, Phys. Rev. B **85**, 104504 (2012).
[6]T. Haugan, P. N. Barnes, R. Wheeler, F. Meisenkothen, and M. Sumption, Nature **430**, 867 (2004).
[7]A. Snezhko, T. Prozorov, and R. Prozorov, Phys. Rev. B **71**, 024527 (2005).
[8]L. N. Bulaevskii, E. M. Chudnovsky, and M. P. Maley, Appl. Phys. Lett. **76**, 2594 (2000).
[9]M. Menghini, R. B. G. Kramer, A. V. Silhanek, J. Sautner, V. Metlushko, K. De Keyser, J. Fritzsche, N. Verellen, and V. V. Moshchalkov, Phys. Rev. B **79**, 144501 (2009).
[10]A. García-Santiago, F. Sánchez, M. Varela, and J. Tejada, Appl. Phys. Lett. **77**, 2900 (2000).
[11]K. T. Lau, S. Y. Yahya, and R. Abd-Shukor, J. Appl. Phys. **99**, 123904 (2006).
[12]Y. Zhao, C. H. Cheng, and J. S. Wang, Supercond. Sci. Technol. **18**, S43 (2005).
[13]T. Zhao, A. Scholl, F. Zavaliche, K. Lee, M. Barry, A. Doran, M. P. Cruz, Y. H. Chu, C. Ederer, N. A. Spaldin, R. R. Das, D. M. Kim, S. H. Baek, C. B. Eom, and R. Ramesh, Nature Mater. **5**, 823 (2006).
[14]T.-J. Park, G. C. Papaefthymiou, A. J. Viescas, A. R. Moodenbaugh, and S. S. Wong, Nano Lett. **7**, 766 (2007).
[15]Y. B. Zhang, D. F. Zhou, Z. X. Lv, Z. Y. Deng, C. B. Cai, and S. P. Zhou, J. Appl. Phys. **107**, 123907 (2010).
[16]E. A. Early, C. C. Almasan, R. F. Jardim, and M. B. Maple, Phys. Rev. B **47**, 433–441 (1993).
[17]P. A. Lee, Rev. Mod. Phys. **78**, 17 (2006).
[18]D. Marconi, M. Pop, and A. V. Pop, J. Alloys Compd. **513**, 586 (2012).
[19]P. A. Lee and T. V. Ramakrishnan, Rev. Mod. Phys. **57**, 287 (1985).
[20]P. N. Vishwakarma and S. V. Subramanyam, Philos. Mag. **87**, 811 (2007).
[21]B. Abeles, H. L. Pinch, and J. I. Gittleman, Phys. Rev. Lett. **35**, 247 (1975).
[22]E. Simanek, Solid State Commun. **40**, 1021 (1981).
[23]W. L. Macmillan, Phys. Rev. B **24**, 2739 (1981).
[24]A. I. Larkin and D. E. Khmel'nitskii, Zh. Éksp. Teor. Fiz. **83**, 1140 (1982) [Sov. Phys. JETP **56**, 647 (1982)].
[25]H. F. Hess, K. de Conde, T. F. Rosenbaum, and G. A. Thomas, Phys. Rev. B **25**, 5578 (1982).
[26]P. N. Vishwakarma and S. V. Subramanyam, J. Appl. Phys. **100**, 113702 (2006).
[27]M. Tinkham, *Introduction to Superconductivity*, 2nd ed. (Dover, 2004); L. G. Aslamazov and A. I. Larkin, Phys. Lett. A **26**, 238 (1968).
[28]N. A. Khan, N. Hassan, S. Nawazj, B. Shabbir, S. Khan, and A. A. Rizvi, J. Appl. Phys. **107**, 083910 (2010).
[29]G. Balestrino, M. Marinelli, and E. Milani, Phys. Rev. B **46**, 14919 (1992).
[30]W. Lang and G. Heine, Phys. Rev. B **51**, 9180 (1995).
[31]W. E. Lawrence and S. Doniach, in *Proceedings of the Twelfth International Conference on Low Temperature Physics*, edited by E. Kanda (Keigaku, Tokyo, 1971), p. 361.
[32]Q. Y. Ying and H. S. Kwok, Phys. Rev. B **42**, 2242 (1990); X.-F. Chen, M. J. Marone, G. X. Tessema, M. J. Skove, and M. V. Nevitt, Phys. Rev. B **48**, 1254 (1993).
[33]R. Seto, R. Botet, and H. Kuratsuji, Phys. Rev. B **73**, 012508 (2006).
[34]P.G. Degennes, Rev. Mod. Phys. **36**, 225 (1964).
[35]P. G. De Gennes, Phys. Lett. **5**, 22 (1963).
[36]V. Ambegaokar and A. Baratoff, Phys. Rev. Lett. **10**, 486 (1963).
[37]A. A. Golubov, E. P. Houwman, J. G. Gijsbertsen, V. M. Krasnov, J. Flokstra, H. Rogalla, and M. Yu. Kupriyanov, Phys. Rev. B. **51**, 1073 (1995).
[38]H. Hilgenkamp, Rev. Mod. Phys. **74**, 485 (2002).
[39]P. Chaddah, Sadhana **28**, 273 (2003).